Single layer porous media with entrapped minerals for microscale studies of multiphase flow

Rinse Liefferink, Antoine Naillon, Daniel Bonn, Marc Prat, Noushine Shahidzadeh

Single layer porous media with entrapped minerals for microscale studies of multiphase flow

R. W. Liefferink, *[a] A. Naillon,[bc] D. Bonn, [a] M. Prat[b] and N. Shahidzadeh[a]

The behaviour of minerals (*i.e.* salts) such as sodium chloride and calcite in porous media is very important in various applications such as weathering of artworks, oil recovery and CO_2 sequestration. We report a novel method for manufacturing single layer porous media in which minerals can be entrapped in a controlled way in order to study their dissolution and recrystallization. In addition, our manufacturing method is a versatile tool for creating monomodal, bimodal or multimodal pore size microporous media with controlled porosity ranging from 25% to 50%. These micromodels allow multiphase flows to be quantitatively studied with different microscopy techniques and can serve to validate numerical models that can subsequently be extended to the 3D situation where visualization is experimentally difficult. As an example of their use, deliquescence (dissolution by moisture absorption) of entrapped NaCl crystals is studied; our results show that the invasion of the resulting salt solution is controlled by the capillary pressure within the porous network. For hydrophilic porous media, the liquid preferentially invades the small pores whereas in a hydrophobic network the large pores are filled. Consequently, after several deliquescence/drying cycles in the hydrophilic system, the salt is transported towards the outside of the porous network *via* small pores; in hydrophobic micromodels, no salt migration is observed. Numerical simulations based on the characteristics of our single layer pore network agree very well with the experimental results and give more insight into the dynamics of salt transport through porous media.

Introduction

Fluid, solute and particle transport processes through porous media are encountered in a wide range of applications such as oil recovery,[1] solute and colloidal transport in soils,[2] salt crystallization in oil reservoirs,[3] carbon storage,[4] building materials[5–7] and artwork.[8,9] For example, the quantification of the acid dissolution of carbonate rocks in reservoirs is a major issue.[10,11] On the other hand, salt transport and crystallization on the pore scale can lead to reduction of porosity and permeability.[3,4] This can result in severe mechanical damage to buildings and artworks.[5–9,12] The kinetics of the flow and transport are often driven by the wetting and the physical properties of porous media such as pore size and surface properties. Since porous media encountered in nature and many applications typically have small pore sizes, for most practical purposes the effect of gravity may be neglected and surface forces such as surface tension, electrostatic and van der Waals forces and surface roughness become important parameters. As a direct consequence, microscale approaches are needed to study liquid and solid transport in small volumes. It is only if one can follow the transport phenomena that experimental results can be integrated into computational approaches to maximize their joint predictive capabilities in terms of parameter space and up-scaling. Generally, this is difficult in 3D porous media because the samples are not transparent and 3D tomography, which, although an important tool, is not easily accessible, limited in resolution and time-consuming.[13,14] There is therefore an urgent need to develop micro/nanoscale experimental devices in which capillary forces dominate the effects of gravity and inertia and that allow direct monitoring of the dynamics *e.g.* using a microscope.[4,10,15,16]

Here, we report novel quasi-2D micromodels of porous media in which the transport of fluids and the interaction with minerals in the porous network can be studied directly using microscopy techniques. The novelty of our work is that we are able to fabricate consolidated microporous materials with only a single layer of microbeads with entrapped salts or controlled pore size distribution. Although Hele–Shaw cells with unconsolidated beads have been used previously,[17–19] we manufacture robust miniature cells which, due to consolidation, do not change under pressure or flow. These model systems can be washed and used several times for different

[a] *Institute of Physics, University of Amsterdam, Science Park 904, 1098 XH Amsterdam, The Netherlands. E-mail: r.w.liefferink@uva.nl*

[b] *Institut de Mécanique des Fluides de Toulouse, IMFT, Université de Toulouse, CNRS - Toulouse, France*

[c] *Laboratoire Rhéologie et Procédés, Quai de France, F-38041 Grenoble, France*

types of experiments with various microscopy techniques such as confocal, inverted microscopy, X-ray micro-tomography, *etc.* The advantages of this strategy are that we can fabricate/study: a) salt entrapped in model porous media and b) model porous media with multiple pore size distributions. This allows us to fabricate bimodal/or even multimodal 2D sintered microglass bead porous media by using salt in the fabrication process and by controlling the size of salt crystals and their location; bimodal/multimodal model porous media fabrication, similar to real stones in 2D, is a challenging problem. The creation of large pores by putting salt grains is unique and is only possible in our consolidated system (in an unconsolidated packing of beads, local bead rearrangements after dissolution of the salt could lead to the filling of the large pores with beads) which can be used in a broad range of applications: 1) when salt is trapped in the porous network, we can use this to study the interaction of minerals with moisture, water and their recrystallization kinetics, 2) when salt is removed, the bimodal/multimodal porous media obtained can be used for different types of 2 phase flow experiments, for example studying water/oil displacement or drying experiments of saturated medium (see Fig. 11 in the Appendix), 3) these microsystems can be used to study the importance of liquid films in the transport processes, under confocal inverted microscopy and micro-tomography techniques. In this short paper, using these micromodels, we investigate the important problem of salt transport through porous media, to show the power of the method. Moisture uptake due to salt is a driving factor in the long-term mechanical deterioration of not only stones but also canvas paintings, as is also responsible for a number of physico–chemical degradation processes in porous artworks such as tiles and sculptures.[9,13,20]

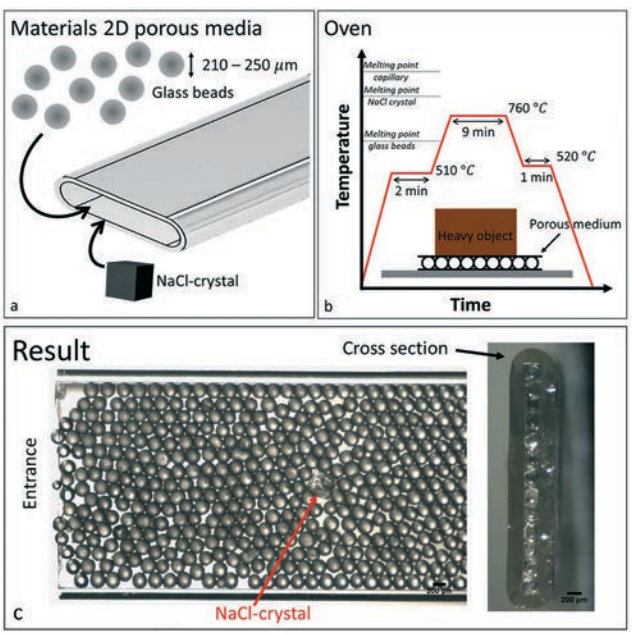

Fig. 1 Schematic representation of the fabrication of 2D porous media. (a) A rectangular capillary was filled with a monolayer of glass beads together with a single NaCl crystal. (b) The sample was placed in an oven where the temperature was increased with a rate of 500 °C h^{-1}, according to a program established in our lab. To achieve contact between the beads and both sides of the capillary, a heavy object (with a pressure of around 50 kPa) was placed upon the sample to decrease the height of the capillary. (c) (left) A representative porous medium, also used for the deliquescence process for hydrophilic 2D porous media. (right) A cross-section of the porous media, used to define the height of the porous network.

Salts that are entrapped in porous materials used for the construction of buildings, outdoor sculptures, and artworks and in soils are ubiquitous and can come from different origins. With environmental fluctuations and cycles of dissolution/deliquescence, salt solution is subsequently mobilized in the pore network and can recrystallize in another location when the relative humidity decreases; this then can cause different types of physical and mechanical weathering.[13] Clearly, the kinetic pathways of dissolution and salt recrystallization strongly influence the way in which different salts cause damage under different environmental conditions. Hygroscopic salt can capture the moisture in air when the relative humidity exceeds the equilibrium relative humidity above a saturated solution and condenses the water vapour into liquid.[21] Despite its importance, little is known about the way salt is mobilized and transported; the kinetics of moisture absorption and recrystallization of entrapped salts has so far not been studied on the pore scale because it is experimentally very challenging. Having entrapped salt in a controlled way in micromodels of a porous media network is not an easy task and consequently quantitative studies on the pore scale remain scarce. Our novel micromodel allows salt crystals to be entrapped in a controlled way to study the absorption of water vapour, the dissolution rate of the crystal phase and the fluid transport of the brine solution within the porous network with different wetting properties. The experimental results are compared with numerical simulations using a pore network model with the geometrical and wetting characteristics of the porous medium used in experiments. These results can serve to validate numerical models that can subsequently be extended to the 3D situation, where visualization experiments are difficult.

Materials and method

A rectangular microcapillary (Vitrocom, borosilicate, 52 × 52 × 0.3 mm^3) was filled with soda lime glass beads (Polysciences, diameter of 210–250 μm, melting point 710 °C), see Fig. 1a. To achieve a well-packed bead arrangement, the microcapillary was centrifuged (4000*g*, 25 minutes) and, if necessary, filled with some more and centrifuged again. While loading the capillary with the glass beads, small NaCl crystals (50.5 μg, Sigma Aldrich), with a similar size to the glass beads, were placed manually at a desired location. This is what we have done for our deliquescence experiment; we put only one single crystal at a controlled distance of 4 mm from the entrance. In addition, the size of the salt crystal can also be controlled by evaporating a known volume of salt

solution. The filled capillary is subsequently sintered by following the 4 steps described in Fig. 1b. The sample is heated near the glass transition temperature (630–650 °C) so that the glass beads soften and sinter together by forming bridges without deforming their overall shape; the salt crystals will stay entrapped as their melting temperature becomes much higher (approximately 800 °C). To ensure a good contact of the glass beads with the wall of the capillary, a load (1 kg) is placed on top of the sample during the sintering process (Fig. 1b). Upon cooling, a consolidated quasi-2D porous material of sintered microglass beads with entrapped salt crystals is obtained. The method can be applied to any salt with a melting temperature higher than approximately 650 °C. We have used monodisperse 230 μm beads, but the process can also be applied to smaller beads. The final height of the porous media is determined by taking an image of the cross-section of the capillary at the end of sintering; the latter is typically on the order of 200–240 μm. The use of NaCl as the salt crystal enables also fabrication of porous media with a controlled bimodal pore size distribution. After sintering, the entrapped NaCl crystals can be removed by simply washing the sintered porous network with water. This leaves large holes at the places where the salt crystals were placed, in addition to the smaller pores that were already present between the sintered beads, see Fig. 10 in the Appendix for an example.[22,23] Of course, we can also directly pre-mix varying proportions of glass beads and salt in order to change the overall porosity of the sintered porous network in a controlled way but with a random distribution of large pores. The 2D porous network with such controlled bimodal porosity can also be used for various experiments of multiphase flow. Knowing the height h, the porosity of the network is determined using image analysis. From the images with area A, we can count the number of sintered beads N_b with sizes d. Therefore, we can determine the porosity using the following equation:

$$\phi_g = 1 - \frac{1}{6}\pi d^3 \frac{N_b}{hA} \quad (1)$$

For the bimodal porous media (after washing the salt), in addition to the way described above, the global porosity was also defined by weighing the sample before and after saturation with water. In this way, we have made samples with up to 50% porosity to simulate stones such as Maastricht limestone that has a porosity of around 50%.

The sintered network, generally hydrophilic, was also treated by silanization with Dynasylan F 8261 as described earlier in ref. 24 to make a hydrophobic one. The wetting properties of the 2D porous media, both hydrophilic and hydrophobic, are determined independently at the pore level by measuring the contact angle θ of a capillary bridge of water between a glass bead and a glass plate. This results in a contact angle of θ = 7° for the untreated porous medium and 108° after silanization (see Fig. 12 in the Appendix). We consider full wetting of the liquid with the salt crystal.[25] This 2D models with entrapped minerals can be used to study the flow and dissolution process in various applications.

When the salt is left in the quasi-2D porous media, this system can be used to study how salt is mobilized in stones. To do so, our porous network, where one entrance is blocked using epoxy glue, is placed horizontally in a controlled miniclimatic chamber with a controlled relative humidity RH ~80%, which is higher than the equilibrium relative humidity above a saturated NaCl solution (RH_{eq} ~75%). The experiments are conducted horizontally, *i.e.* perpendicular to gravity to avoid the influence of buoyancy flows. Using an optical microscope coupled to a CCD camera, we can then monitor the water vapour absorption by the salt crystal; water will start to form around the hygroscopic crystal and slowly dissolve it. We monitor the evolution of the liquid–air and liquid–crystal interfaces in time to quantify the deliquescence rate of the crystal and the pore invasion dynamics. After complete deliquescence of the salt, the relative humidity of the chamber is decreased (RH ~6%) and the evaporation of the entrapped salt solution is monitored until complete drying and salt recrystallization.

We use a pore network model to simulate the experimental results of deliquescence in the 2D porous media. The simulations were based on the algorithms of Straubhaar and Prautzsch[26,27] which were modified to the specific case of deliquescence. The geometry of the pore network used in the simulations is based on the average pore volume, porosity and lattice spacing that correspond to the two regions in the experimental porous media; we have distinguished two types of regions since the visual inspection of the micromodel clearly shows regions of more compact packing and regions of less compact packing. For simplicity, we use a 2D square network; the pores are the intersection of the channels, where the throats are the connection between the pores (Fig. 2 and inset). The sizes of the elements are distributed (normal distribution, average standard deviation of 10%) in the in-plane dimensions (where the height is taken as a

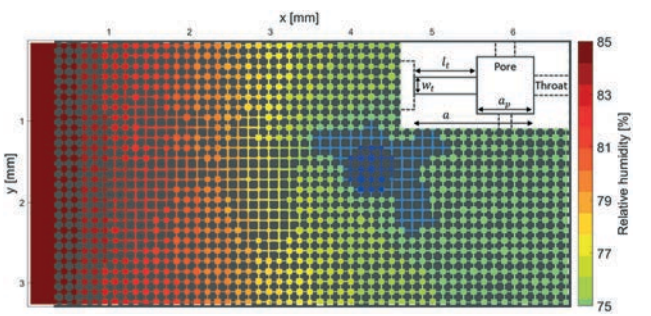

Fig. 2 Realization of the pore network model based on the specific geometry of the 2D hydrophilic porous medium experiment after 6 h. The dark blue and blue colours represent respectively the crystal and liquid phase. Inset: Schematic representation of a single pore in the square network. The pore with size a_p is connected to 4 throats with different widths w_t and lengths l_t. The depth (out-of-plane) of throats and pores and the lattice spacing are constant throughout the network.

constant over the full network). However, the element dimensions have a few restrictions: a) the sizes should always result in the set lattice spacing a, b) the sizes should always be larger than zero, and c) the sizes in the two regions should not overlap. Afterwards, the mass flux of the water vapour towards the liquid cluster is computed, by considering the distribution of the water vapour in the network as a quasi-steady state, without convection (see Appendix for details). The invasion of new elements in the network is based on the capillary pressure and local invasion rules, which depend on the wettability of the network.[28] It should be noted that the invasion rules do not depend on the exact range of throat/pore sizes; the invasion is controlled by the existence of a hierarchy in the throat size so that it is not crucial to impose the exact distribution. The computational time step is based on the invasion time of one new element together with the dissolution of the crystal phase. After each invasion, the water vapour transport and vapour flow towards the cluster are updated. Another important point is the effective diffusion coefficient of the vapour that varies with porosity, which was also taken into account. During the simulation, the time evolution of the total crystal mass m_c, liquid volume V_l, location of the liquid cluster and the concentration field are analysed (*e.g.* see Fig. 2). Because the sizes of pores and throats are based on a normal distribution, the kinetics used in the results are taken as an average of 5 simulations on 5 different realizations of the pore network.

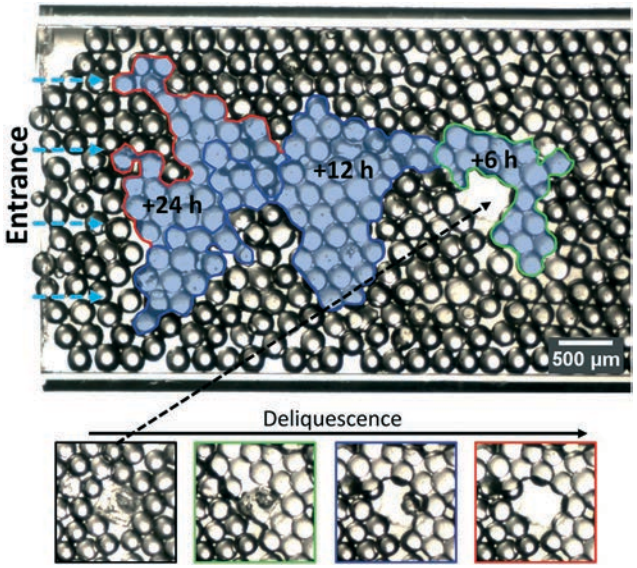

Fig. 3 Microscopy image for hydrophilic 2D porous medium after deliquescence. Vapour has entered the porous media from the left, is absorbed by the NaCl crystal (which was located in the big pore) and consequently dissolves the crystal in the given final brine solution. The areas marked in green, blue and red represent the evolution of the liquid clusters after 6 h, 12 h and 24 h. Below, the images show the crystal corresponding to the marked liquid clusters.

Results and discussion

Deliquescence of entrapped salt

The kinetics of deliquescence of entrapped NaCl crystals is monitored in time for both hydrophilic and hydrophobic 2D porous media. For the hydrophilic 2D porous medium, the entrapped NaCl crystal is located at a distance of 4.5 mm from the entrance at RH = 85 ± 2% and T = 22 °C. When the relative humidity is above 75%, the deliquescence of the salt induces the formation of a salt solution at saturation; the salt crystal absorbs water to dissolve and there is no salt deposition because there is no evaporation at this stage. In Fig. 3 the microscopy images of moisture absorption by the salt crystal (24 h) are shown. Due to the refractive index difference between water and air, the location where salt solution is present can be observed in the image as well as the liquid–air interface (see Fig. 13 in the Appendix). The salt solution invades the pores on top of each other that are connected simultaneously. No difference was found at different depths of view. In Fig. 3 the colours green, blue and red represent the growth of the salt solution cluster after 6 h, 12 h and 24 h respectively to emphasize the volume evolution with time and the final salt solution volume. We can observe that the deliquescence of the crystal phase results in the invasion of the salt solution in the neighbouring pores. The salt solution invades the smaller pores, *i.e.* the close-packed glass bead region in the porous network where the maximal capillary pressure can be found (see also Fig. 13 in the Appendix for the difference in pore sizes and packing of glass beads). This is expected from considering the capillary pressure associated with each element in the network:

$$\Delta P = \frac{4\gamma\cos\theta}{d_c} \tag{2}$$

where γ is the surface tension and d_c is the element size. Since the driving pressure for invasion is larger in smaller pores, the latter are the first to be invaded.

With the use of image analysis, knowing the height of the capillary and the porosity of the densely packed region (ϕ = 33.1%), the time evolution of the total volume of the salt solution can be determined. The porosity of 33.1% for the close-packed region is based on the minimal porosity of a close packing structure. For a perfect arrangement of beads, the porosity can be calculated with the use of a geometrical argument, depending on the known diameter of beads and height of the microcapillary. As shown in the figures above, the beads are not significantly deformed; in addition, a small deformation of the beads will not change their volume and hence the porosity is not changed. The uncertainty is based on systematic experiments measuring the porosity from images and from saturation with water and weighing. As can be observed in Fig. 4 (red circles), the time evolution exhibits two regimes. In the first regime (until 20 h), we observe the deliquescence of the crystal, and the volume of the salt solution increases almost linearly in time. In the second regime which corresponds to the stage where the crystal is

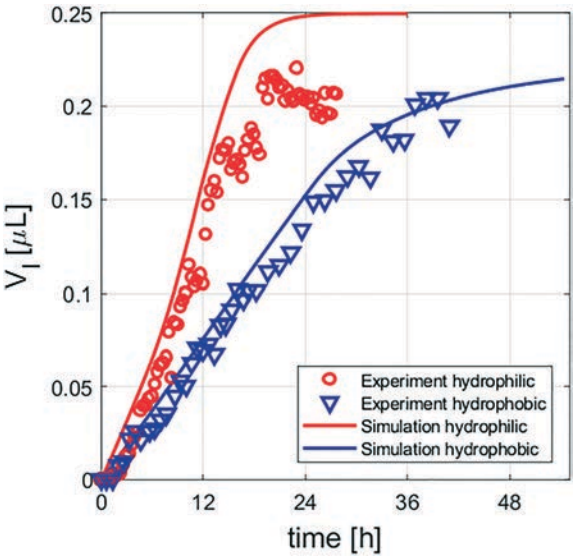

Fig. 4 The volume V_l of the salt solution in time for the 2D hydrophilic (red) and hydrophobic (blue) porous media and pore network models. The volume increases until the crystal is totally dissolved (hydrophilic after 13.75 h and hydrophobic after 29.5 h); subsequently the solution increases slowly and the salt concentration decreases until a constant salt solution volume is reached. The equilibrium state corresponds to a salt solution at the concentration corresponding to the equilibrium water vapour pressure fixed by the RH of the climatic chamber.

completely dissolved (13.75 h), the water vapour absorption rate decreases and a constant volume is reached. This equilibrium state corresponds then to a salt solution with a concentration corresponding to the equilibrium water vapour pressure fixed by the RH of the climatic chamber.

For the hydrophobic porous medium (Fig. 5), the salt crystal was located at a distance of 3.8 mm from the entrance and exposed to RH = 83 ± 2% and T = 22 °C. In contrast to what was observed for the hydrophilic porous medium, the resulting salt solution preferentially invades the large pores rather than the smaller ones. In the hydrophobic medium, the contact angle is high and the liquid–air interface curvature leads to a negative capillary pressure; for the large pores, this negative pressure is smaller and consequently the liquid will spontaneously invade the large pores. The time evolution of the liquid volume is given in Fig. 4 (blue triangles); although a similar initial linear trend to that for the hydrophilic network is found here, the deliquescence rate in the hydrophobic medium is significantly slower than for the hydrophilic case. This can be understood in terms of the diffusion length, which is the distance between the entrance of the capillary and the liquid–air interface, the distance that the water vapour should diffuse through. In the hydrophilic porous medium, the liquid invades the pores towards the entrance, and consequently the diffusion length is reduced. In the hydrophobic porous medium, the distance does not decrease; the liquid invasion occurs on the big pores around the location of the salt. Therefore, the deliquescence rate is slower compare to that in the hydrophilic porous medium.

The kinetics of the deliquescence in these quasi-2D porous networks is modeled using the pore network model, by considering the hydrophilic and hydrophobic characteristics and taking the environmental conditions into account. In Fig. 4 the growth of the liquid pocket in time is shown with a continuous line; the initial growth rate of the salt solution volume is in very good agreement with the obtained experimental results. However, for the hydrophilic network, the speed of the moisture absorption and the final liquid volume plateau remain slightly higher than the experimental results. The uncertainty on different parameters can be at the origin of this discrepancy such as the uncertainty on the crystal mass or relative humidity, and possibly on the ion concentration gradients induced in the salt solution during the increase of the volume of the salt solution; in fact, in our simulations, we consider that the resulting salt solution is in equilibrium with the crystal during the whole process.

In order to check the impact of the concentration gradients, we have completed these 2D network experiments by some experiments of 1D deliquescence of a NaCl crystal (12.1 μg) entrapped in a square microcapillary (100 μm) where one of the two sides is sealed, as a model for a single pore. These experiments were performed at RH = 80 ± 2% and T = 23 °C. Fig. 6 shows representative images before and after 5 h of moisture absorption. We have recorded the evolution of the distance δ of the liquid–air meniscus from the entrance of the capillary in time, see Fig. 7 (black squares). An analytical

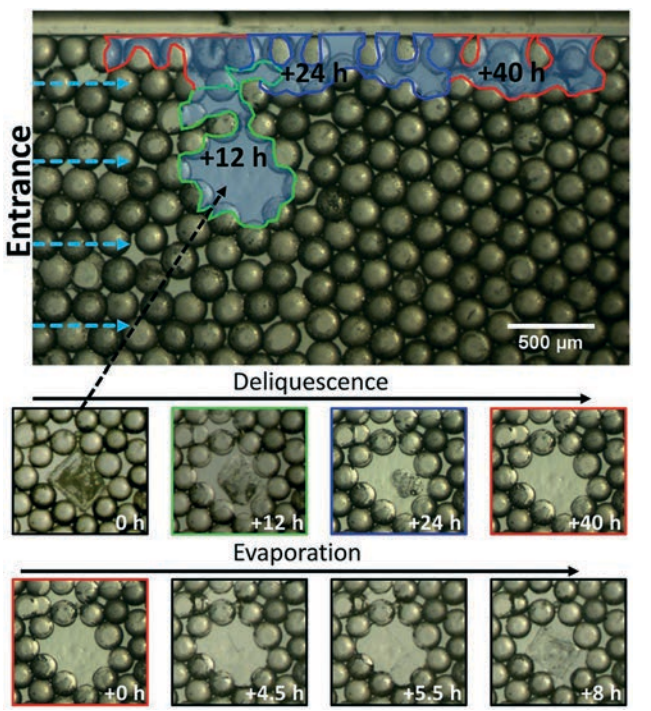

Fig. 5 Microscopy image for the hydrophobic 2D porous medium after deliquescence. The areas marked in green, blue and red represent the evolution of the liquid clusters after 12 h, 24 h and 40 h. Below, the images show the crystal during the deliquescence (first row) and evaporation (second row) processes. The drying process results in a reversed process of the crystal.

model was then made to describe the moisture absorption as a pure diffusion equation. The water vapour flux density e at the liquid–air interface can be written as:[29]

$$e = -\rho_g D \frac{\Delta\omega}{\delta + \delta_{ext}} \quad (3)$$

where ρ_g is the density of the gas, D the vapour diffusion constant in the gas, $\Delta\omega = \omega_i - \omega_\infty$ the difference in water vapour mass fraction above the NaCl solution (ω_i) and at the entrance of the microcapillary (ω_∞, $RH_\infty \approx 80\%$) and δ_{ext} the external transfer length, *i.e.* the diffusion length between the entrance of the tube and the external controlled gas. The external transfer length is on the order of the tube size and therefore δ_{ext} = 100 μm.[30] If we assume that a homogeneous saturated salt solution is formed due to the water vapour absorption and dissolution of the crystal, the distance of the meniscus from the entrance of the capillary (*i.e.* the water vapour path length) can be written as:

$$\delta(t) = \sqrt{2D\rho_g\Delta\omega\left(\frac{m_0+1}{\rho_{sol}} - \frac{m_0}{\rho_c}\right)t + \left(\delta_0 + \delta_{ext}\right)^2} - \delta_{ext}. \quad (4)$$

where m_0 is the saturated salt concentration (in molality), ρ_{sol} the density of the solution at saturation, ρ_c the crystal phase density and δ_0 the initial length at $t = 0$. Fig. 7 shows that the vapour diffusion model (red dashed line) agrees very well with the experiment up to 20 h. For longer deliquescence time, the model overestimates the moisture absorption, resulting in a smaller δ after 20 h in a shorter time; *i.e.* the salt solution becomes closer to the entrance more quickly. As confirmed by numerical simulations (see below), this deviation is possibly due to the increased role of advection relative to the diffusion of ions in the liquid plug of salt solution. We have calculated the Peclet number (the ratio of advective to diffusive transport), which is shown in the inset of Fig. 7. Pe can be calculated from $\mathrm{Pe}(t) = -\frac{l_l(t)}{D_s}\frac{\mathrm{d}\delta(t)}{\mathrm{d}t}$ where $l_l(t)$ is the length of the salt solution plug and $D_s = 8.3 \times 10^{-10}$ m^2 s^{-1} is

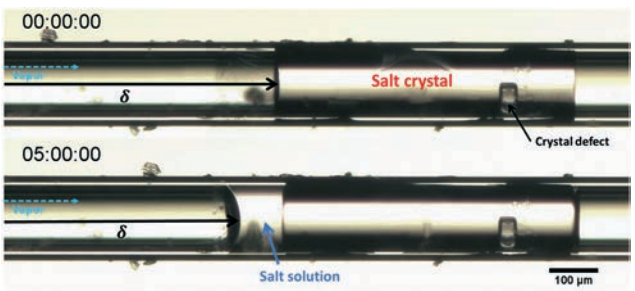

Fig. 6 Representative image of the deliquescence of a NaCl crystal in a microcapillary. From the open left side, air with a relative humidity of 80% enters the pore inducing the deliquescence of the hygroscopic salt by forming a salt solution at almost saturated salt concentration.

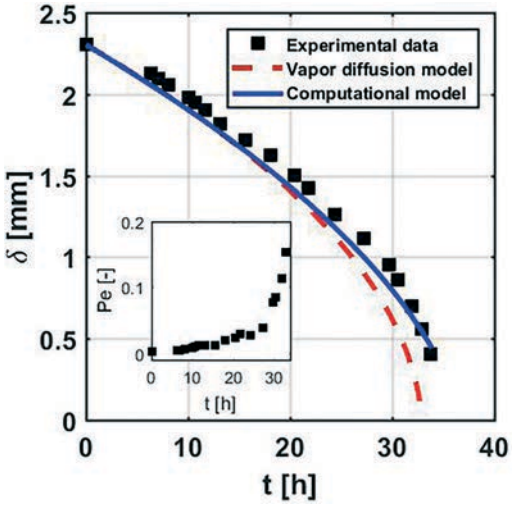

Fig. 7 The length δ from the liquid–air interface to the entrance in time. The decrease of δ in time is based on the displacement of the liquid–air meniscus, the growth of the liquid phase, towards the entrance. In black squares, the experimental data are given which were modeled with a vapour diffusion model (red dashed line) and a computational model (blue line) where the salt diffusion through the liquid phase was computed. In the inset, the Peclet number (the ratio of advective to diffusive transport) in time is given where a sharp increase is visible when the vapour flux is increased due to a small diffusion length δ.

the diffusion coefficient of salt at saturation. It indeed shows a sharp increase after 20 h: when the meniscus becomes closer to the entrance of the capillary, the salt solution becomes more heterogeneous and a salt concentration gradient starts to appear.

In order to model the deliquescence process in the presence of a salt concentration gradient, full computation of the vapour diffusion combined with the salt diffusion and advection in the liquid phase was performed. Using the finite-element code Comsol®, we compute the vapour- and salt mass transfer equation combined with dissolution of the crystalline phase (with a rate of $k_r = 2.3 \times 10^{-3}$ m s^{-1} using a formula quite similar to the one presented in Appendix D in the work of Naillon *et al.*[31]). As can be observed in Fig. 7 (blue line), the result obtained with this model describes the full deliquescence process very well till the very end of the process. Our results show that after 30 h, the salt concentration at the liquid–air interface decreases to $m_i = 0.93m_0$ (m_0 being the saturation concentration close to the crystal phase). This induces an increase of the equilibrium RH from 75%, for the solution at saturation, to 77% above the undersaturated salt solution.

To support the analogy between the tube experiment and the porous medium, we have computed the Peclet number in our sintered bead porous network. Considering for simplicity the growing liquid cluster as a liquid plug of width W, thickness h and length $L(t)$, the Peclet number can be expressed as a function of $\mathrm{d}V_l/\mathrm{d}t$ (see Appendix for more details). Then from the slope of the curves in Fig. 4, the estimate of the Peclet number leads to values in the same range as for the

capillary tube. We find that Pe ≈0.05–0.13, which is fully in the range of the Peclet number where the convective effect is non-negligible. These results then provide the explanation as to why experimentally a lower moisture absorption rate is detected compared to the simulation in the second regime of the deliquescence process.

Deliquescence/drying cycles

After complete deliquescence, the brine solution is evaporated at a controlled relative humidity of RH = 6 ± 2% till recrystallization of the salt. In the hydrophilic 2D network, the drying occurs first in the large pores, followed by the small ones. This is expected based on the capillary pressure and the invasion of air as the non-wetting fluid. The water evaporation leads to the formation of several disconnected liquid clusters in the porous network; their further evaporation induces crystallization of the salt as several tiny microcrystallites in different locations as can be seen in Fig. 8. These are on average closer to the entrance of the capillary than where the initial entrapped crystal was located. Clearly, the deliquescence, followed by drying, transports the salt towards the entrance *via* the smaller pores. This phenomenon takes place mainly due to the convective ion transport in the liquid cluster during drying. Since the relative humidity is only 6%, the Peclet number is much larger compared to that of the deliquescence process (see also the difference in the time scale of the deliquescence and drying in Fig. 5). This results in the preferential formation of the crystals in the region of the cluster closest to the entrance (because the ions accumulate where the evaporation flux is greatest due to the convective effect). This is likely to eventually lead to the efflorescence of the salt after several cycles: the salt comes out of the pores. This is in fact a common observation for NaCl entrapped in porous media, which is frequently visible as a white deposit coming out of bricks and stones on buildings

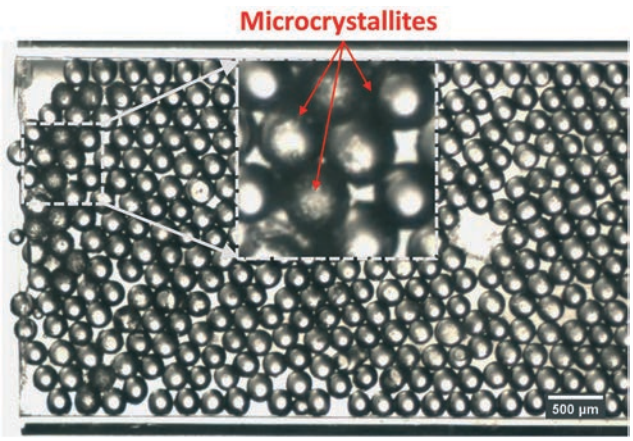

Fig. 8 Microscopy image for the hydrophilic 2D porous medium after 4 h of drying (RH = 6 ± 2%) which followed after the deliquescence process (see Fig. 3). The big pore, where the salt crystal was initially entrapped, is empty. Several tiny microcrystallites are found towards the entrance, which are also visible in the zoomed-in inset.

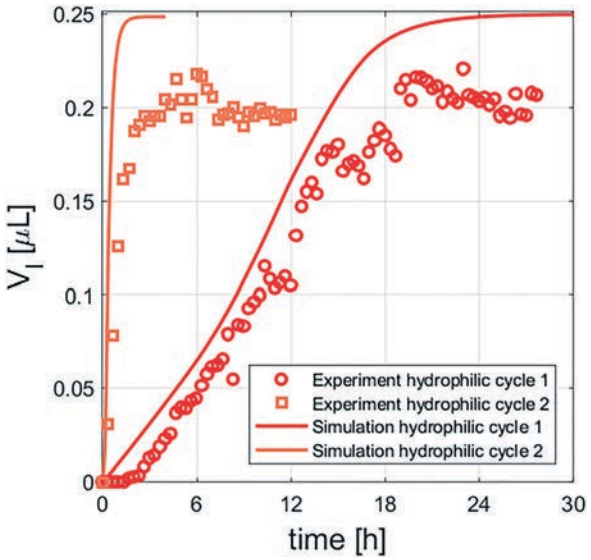

Fig. 9 The volume V_l of the salt solution in time for the 2D hydrophilic porous medium and pore network model for the first cycle (red) and second cycle (orange). In the second cycle, based after drying and recrystallization processes, multiple microcrystals are located close to the entrance which results in an 8 times faster deliquescence process compared to the first cycle.

and statues.[13] To confirm this, a second cycle of deliquescence/drying is imposed on the sample. The moisture absorption and the growth of salt solution around the microcrystals result in one large liquid pocket that forms close to the entrance of the capillary. In Fig. 9 (orange squares). For the same amount of salt, the deliquescence rate becomes 8 times faster than the first cycle. The result shows that the deliquescence of a large number of tiny microcrystals is much faster than that of a single large crystal because of their much larger surface area. Moreover, because these microcrystals are located closer to the entrance, the moisture absorption can then start earlier in time. The numerical simulations based on the location of the microcrystals as found after drying are given as the orange line in Fig. 9 and agree very well with the experimental results.

The drying of the hydrophobic porous network shows again exactly the opposite behaviour compared to the hydrophilic medium: after a first complete deliquescence cycle, the drying and the invasion of air (RH = 6 ± 2%, here as the wetting fluid) start in the small pores and lead to the recrystallization of the salt in the largest pore, *i.e.* the pore where the crystal was located before the deliquescence process. Similar to the deliquescence process, the hydrophobic properties of the porous network result in a negative capillary pressure, and consequently, the air invasion starts in the smallest pores. Therefore, the deliquescence and drying processes lead to a fully reversible recrystallization. At the drying step, air which is now the wetting fluid will invade the small pores first, and consequently with evaporation, the recrystallization occurs rather in the big pores. A second cycle results again in similar liquid invasion and kinetics of recrystallization.

Consequently, no migration of the salt is observed over the deliquescence/drying cycles when the 2D porous medium has a hydrophobic coating.

Conclusions

Moisture is a driving factor in the long-term mechanical deterioration of salt-containing stones and works of art. We have developed novel porous networks, where minerals (such as NaCl, Na_2So_4, $CaCO_3$, $MgSO_4$) can be trapped in a controlled way in single layer porous media in order to follow their behaviour under multiphase flow in the porous network. The advantage of these microporous media is that they can be used for direct and quantitative monitoring of moisture absorption, salt transport and crystal dissolution/recrystallization in porous networks for which the porosity, wetting properties and location of the entrapped salt can be controlled. Our results show that the moisture absorption by the NaCl crystal and the liquid invasion in the porous network is controlled by the wetting properties and the capillary pressure. A positive capillary pressure, in a hydrophilic medium, results in the invasion of the salt solution in the small pores, whereas large pores are invaded preferentially in the hydrophobic medium due to the negative capillary pressure. The moisture absorption rate mainly depends on the vapour diffusion length, *i.e.* the distance between the entrance of the capillary and the liquid–air interface, and the equilibrium vapour pressure above the resulting liquid–air interface which is controlled by the salt concentration gradient. The subsequent drying in hydrophilic medium shows the transport of the salt towards the external surface of the porous materials. On the other hand, in the hydrophobic media the salt crystal reforms at the same location even after several dissolution/drying cycles. Simulations based on a pore network model with the characteristics of our 2D network describe the kinetics well and allow for more insight into the dynamics of moisture absorption due to salt in porous media.

Our novel method of manufacturing miniature microporous media by using microglass beads and salt crystals in the sintering process is also a versatile tool for creating controlled bimodal/multimodal pore sizes with controlled porosity in the range $25\% \leq \phi_g \geq 50\%$. These porous networks either with the entrapped minerals or with bimodal pore sizes can then be used for different experiments of multiphase flow under phase contrast microscopy/confocal microscopy and also for microtomography experiments. In this way, 2D experimental results can then serve to validate numerical models that can subsequently be extended to the 3D situation, where visualization experiments are difficult.

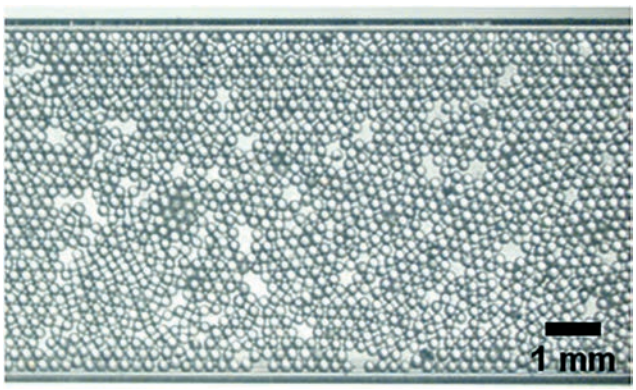

Fig. 10 Microscopy image of a 2D bimodal porous medium, the entrapped crystals are washed out after the sintering procedure.

Appendix

Bimodal porous medium

During the fabrication of 2D porous media, NaCl crystals are used to obtain bimodal porosity. The entrapped crystal can be removed after sintering which leaves large holes. See Fig. 10 for an example.

Two-phase flow in multimodal pore size microporous media

With the use of a single layer porous medium with consolidated packing of beads, two-phase flow experiments can be studied. In the microscopy image in Fig. 11, a multimodal pore size distribution is used where the drying of saturated NaCl solution is monitored. The air-invasion follows the large pore sizes where, due to the connection of the salt solution with the entrance, efflorescence is found at the outer surface of the porous medium.

Contact angle θ

The wetting properties of the hydrophilic and hydrophobic 2D porous media are determined by measuring the contact angle θ. This is the angle between the tangent to the glass bead at the point of contact with the liquid and the line extending the liquid meniscus at this point, see Fig. 12. We consider that the entrapped crystals are not affected by silanisation seeing that the dissolution rate of the treated crystal does not change after silanisation. It is also possible

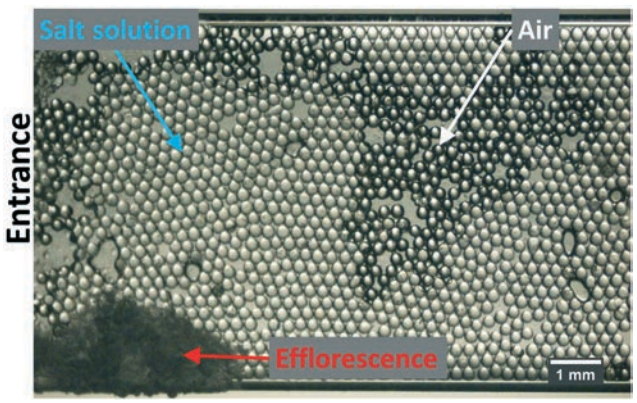

Fig. 11 Microscopy image of a multimodal pore size microporous medium. The porous medium is saturated with NaCl solution at saturation to monitor the drying. The air invasion is followed by subsequent crystallization of the NaCl.

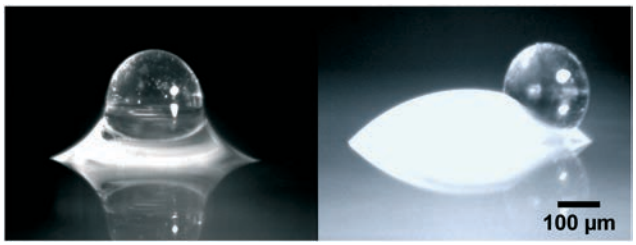

Fig. 12 The wetting for a hydrophilic (left) and hydrophobic (right) glass bead and glass plate.

to change the wetting properties of these networks heterogeneously by partial saturation of the network with a silane solution.

Discrete water vapour transport

To compute the molar field ($X_v = P_v/P_0$) of the moisture, the equations governing the transport of the vapour within the gas regions of the pore network must be solved. Neglecting convective effects and due to the assumption of a quasi-steady state, a steady-state binary diffusion problem is considered. Within the framework of pore network models, the method of solution consists of expressing the diffusion flux Φ_{vij} through a throat along the x-direction between two neighbouring pores i and j according to the finite difference scheme as (a similar formula is made along the y-direction),

$$\Phi_{vij} = -c_g D^* \frac{X_{vj} - X_{vi}}{a} w_t d_t \tag{5}$$

where w_t and d_t are respectively the width and depth of the throat. D^* is a local diffusion coefficient. It is expressed as $D^* = D_v/\tau$ where D_v is the vapour molecular diffusion coefficient and τ is a correction factor taking into account the effect of the local geometry ($\tau = 1$ for a straight tube). Here, τ is determined considering that the two pores are connected by a throat of width w_t and length βa and two half pores of width a and length $(1 - \beta)a/2$. Considering for simplicity $w_t \approx \beta a$, the consideration of this transport problem as the combination of three resistances in series leads to τ expressed as

$$\tau = \frac{(1-\beta)^2 + \beta}{1-\beta} \tag{6}$$

This is an approximation since the factor τ is constant all over the network. The parameter β is specified so as to impose a given porosity ϕ, $\beta = \sqrt{1-\phi}$. In our case, this enables us to take into account the porosity variation between the compact region and the less compact region of the micromodel. Due to mass conservation in each pore, the equation to solve for every pore in the network is:

$$\sum_{j=1}^{4} \Phi_{vij} = 0 \tag{7}$$

with i as the pore of interest and j as the pores connected through throats to i. eqn (7) is used to solve for each pore in the network under the following conditions:

- Inlet channel

To be able to compute the outside vapour, an inlet channel was added, made of three additional rows of pores with a porosity of 100%. The molar fraction of the inlet vapour was set by:

$$X_v = \mathrm{RH}_{out} \frac{P_{vs}}{P_0} \tag{8}$$

where RH_{out} is the controlled relative humidity outside the porous medium and P_{vs} is the saturated vapour pressure.

- Boundary condition

At all boundaries of the porous medium, except for the inlet channel, zero flux is imposed.

- Liquid–air interface

For the liquid and crystal phase a saturated molar fraction X_{vsat} was used during the deliquescence. This will result in a molar fraction comparable to a relative humidity of 75%. All pores and throats with a partial liquid or crystal phase and pores adjacent to these throats are set to the saturated salt molar fraction.

The relative humidity (RH) was calculated afterwards using $\mathrm{RH} = X_v P_0/P_{vsat}$, where the relative humidity in the throats is the average of the adjacent pores.

Pore sizes

The 2D porous medium is based on the packing of beads in a glass microcapillary. Thereby local variation of bead packing results in a distribution of pore sizes. In Fig. 13, the microscopy image of the hydrophilic 2D porous medium

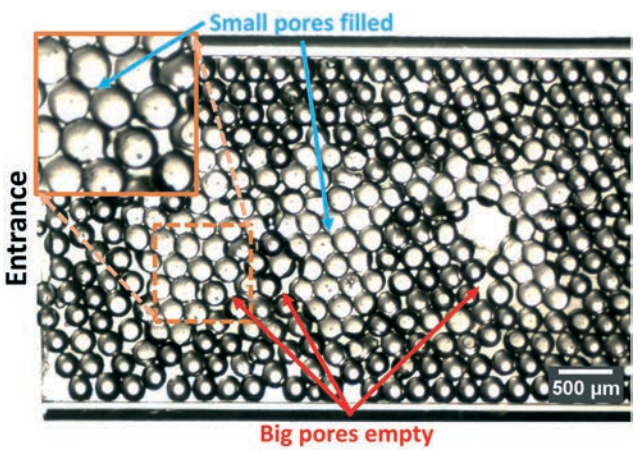

Fig. 13 Microscopy image of the hydrophilic 2D porous medium after deliquescence. During fabrication, local variation of bead packing results in differences of pore sizes. As can be observed, only liquid invasion occurs in the small pores of the hydrophilic porous medium.

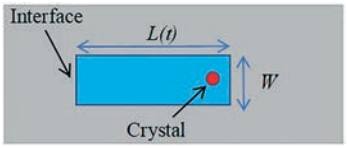

Fig. 14 Schematic description of the deliquescence of a crystal (red circle) forming a liquid cluster (blue) in a 2D porous medium.

after the deliquescence process is given, where the difference in pore sizes is emphasized.

Peclet number for 2D porous media

To estimate the Peclet number in the hydrophilic and hydrophobic 2D porous media as shown in Fig. 3 and 5, the liquid pocket is seen as a liquid plug (in blue) with length $L(t)$ and width W as sketched in Fig. 14 (the crystal corresponds to a red disk). Therefore, the volume of the liquid is:

$$V_l = \phi L(t) W h \tag{9}$$

where h is the height of the micromodel ($h \approx 200$ μm). Neglecting the variation of W, the velocity of the interface is given by:

$$\frac{\mathrm{d}L(t)}{\mathrm{d}t} = \frac{1}{\phi W h}\frac{\mathrm{d}V_l}{\mathrm{d}t} \tag{10}$$

The Peclet number can then be written similar to that for the 1D deliquescence experiment:

$$\mathrm{Pe} = \frac{1}{D_s \phi h}\frac{L(t)}{W}\frac{\mathrm{d}V_l}{\mathrm{d}t} \tag{11}$$

where D_s is the diffusion coefficient of salt at saturation. For the hydrophilic quasi-2D porous medium (see Fig. 3 and 4), we can estimate $\frac{\mathrm{d}V_l}{\mathrm{d}t} \approx 0.15\frac{\mu\mathrm{L}}{12\ \mathrm{h}}$. Furthermore, W varies between 2 and 7 bead diameters, whereas $L(t)$ is approximately equal to 15 bead diameters. If we take $W = 7$ as the average value, then $L(t)/W \approx 15/7$ and therefore Pe ≈0.13, which is fully in the range of the Peclet number where the convective effect is non-negligible according to Fig. 7.

For the hydrophobic quasi-2D porous medium (see Fig. 4 and 5), we can estimate that $\frac{\mathrm{d}V_l}{\mathrm{d}t} \approx 0.15\frac{\mu\mathrm{L}}{24\ \mathrm{h}}$ and $L(t)/W \approx 15/3$. Therefore Pe ≈0.05 which is smaller but still in the range where convection is non-negligible.

Conflicts of interest

There are no conflicts to declare.

Acknowledgements

We thank Jana Prautzsch for using her pore network model as a basis for our version and Mohsin Qazi for developing the fabrication procedure of 2D porous media.

References

1 V. N. Wong, R. C. Dalal and R. S. Greene, *Biol. Fertil. Soils*, 2008, **44**, 943–953.
2 K. Wang, D. E. Nelsen and W. A. Nixon, *Cem. Concr. Compos.*, 2006, **28**, 173–188.
3 Y. Peysson, *Eur. Phys. J.: Appl. Phys.*, 2012, **60**, 24206.
4 M. Kim, A. Sell and D. Sinton, *Lab Chip*, 2013, **13**, 2508–2518.
5 N. Shahidzadeh-Bonn, J. Desarnaud, F. Bertrand, X. Chateau and D. Bonn, *Phys. Rev. E: Stat., Nonlinear, Soft Matter Phys.*, 2010, **81**, 066110.
6 R. M. Espinosa-Marzal and G. W. Scherer, *Acc. Chem. Res.*, 2010, **43**, 897–905.
7 R. J. Flatt, F. Caruso, A. M. A. Sanchez and G. W. Scherer, *Nat. Commun.*, 2014, **5**, 4823.
8 D. D'Agostino, P. M. Congedo and R. Cataldo, *J. Cult. Herit.*, 2014, **15**, 448–457.
9 K. Linnow, L. Halsberghe and M. Steiger, *J. Cult. Herit.*, 2007, **8**, 44–52.
10 W. Song, T. W. de Haas, H. Fadaei and D. Sinton, *Lab Chip*, 2014, **14**, 4382–4390.
11 A. V. Subhas, J. F. Adkins, N. E. Rollins, J. Naviaux, J. Erez and W. M. Berelson, *Proc. Natl. Acad. Sci. U. S. A.*, 2017, **114**, 8175–8180.
12 S. Veran-Tissoires, M. Marcoux and M. Prat, *Phys. Rev. Lett.*, 2012, **108**, 054502.
13 J. Desarnaud, H. Derluyn, L. Molari, S. de Miranda, V. Cnudde and N. Shahidzadeh, *J. Appl. Phys.*, 2015, **118**, 114901.
14 L. Grementieri, F. Daghia, L. Molari, G. Castellazzi, H. Derluyn, V. Cnudde and S. de Miranda, *Int. J. Solids Struct.*, 2017, **126**, 225–239.
15 J. Leng and J.-B. Salmon, *Lab Chip*, 2009, **9**, 24–34.
16 R. Barrett, M. Faucon, J. Lopez, G. Cristobal, F. Destremaut, A. Dodge, P. Guillot, P. Laval, C. Masselon and J.-B. Salmon, *Lab Chip*, 2006, **6**, 494–499.
17 Y. Méheust, G. Løvoll, K. J. Måløy and J. Schmittbuhl, *Phys. Rev. E: Stat., Nonlinear, Soft Matter Phys.*, 2002, **66**, 051603.
18 A. Yiotis, D. Salin, E. Tajer and Y. Yortsos, *Phys. Rev. E: Stat., Nonlinear, Soft Matter Phys.*, 2012, **86**, 026310.
19 N. Sghaier, S. Geoffroy, M. Prat, H. Eloukabi and S. B. Nasrallah, *Phys. Rev. E: Stat., Nonlinear, Soft Matter Phys.*, 2014, **90**, 042402.
20 B. Lubelli, R. P. Van Hees and C. W. Groot, *Constr. Build. Mater.*, 2006, **20**, 691–699.
21 N. Shahidzadeh and J. Desarnaud, *Eur. Phys. J.: Appl. Phys.*, 2012, **60**, 24205.
22 N. Shahidzadeh-Bonn, P. Vié, X. Chateau, J.-N. Roux and D. Bonn, *Phys. Rev. Lett.*, 2005, **95**, 175501.

23 E. Chevalier, D. Chulia, C. Pouget and M. Viana, *J. Pharm. Sci.*, 2008, **97**, 1135–1154.

24 N. Shahidzadeh-Bonn, A. Tournié, S. Bichon, P. Vié, S. Rodts, P. Faure, F. Bertrand and A. Azouni, *Transp. Porous Media*, 2004, **56**, 209–224.

25 T. Corti and U. K. Krieger, *Appl. Opt.*, 2007, **46**, 5835–5839.

26 B. Straubhaar, J. Pauchet and M. Prat, *Int. J. Heat Mass Transfer*, 2016, **102**, 891–901.

27 J. Prautzch, *Master thesis*, ETH Zurich, 2016.

28 L. Ceballos and M. Prat, *Phys. Rev. E: Stat., Nonlinear, Soft Matter Phys.*, 2013, **87**, 043005.

29 B. Camassel, N. Sghaier, M. Prat and S. B. Nasrallah, *Chem. Eng. Sci.*, 2005, **60**, 815–826.

30 F. Chauvet, P. Duru, S. Geoffroy and M. Prat, *Phys. Rev. Lett.*, 2009, **103**, 124502.

31 A. Naillon, P. Joseph and M. Prat, *J. Cryst. Growth*, 2017, **463**, 201–210.